

Line-broadening effects in the powder infrared spectrum of apatite

Etienne Balan · Simon Delattre · Damien Roche · Loïc Segalen · Guillaume Morin · Maxime Guillaumet · Marc Blanchard · Michele Lazzeri · Christian Brouder · Ekhard K. H. Salje

Received: 9 April 2010/Accepted: 12 July 2010/Published online: 10 August 2010
© Springer-Verlag 2010

Abstract The crystallinity of natural and synthetic apatite samples is often determined from the broadening of $\nu_4 \text{PO}_4$ infrared absorption bands. However, various physical mechanisms contribute to the observed linewidth. In the present study, the factors determining the linewidth in the powder spectrum of synthetic fluorapatite and hydroxyapatite samples are investigated. The temperature dependence of the infrared spectrum (10–270 K) is used to assess the respective contributions of homogeneous broadening, related to the decay of phonons through anharmonic coupling, and heterogeneous broadening related to elastic strain and macroscopic electrostatic effects. This latter contribution is dominant in the investigated samples and depends on the shape of powder particles. It is discussed under the light of the theoretical modeling of the low-frequency dielectric properties of apatite based on first-principles density functional theory calculations. The linewidth of the weak $\nu_1 \text{PO}_4$ absorption band provides a reliable information on microscopic sources of broadening, i.e., apatite crystallinity. In comparison, the other more intense PO_4 bands are more sensitive to long-range electrostatic effects.

Keywords Apatite · Infrared spectroscopy · First-principles calculations · Anharmonicity

Introduction

Apatite ($\text{Ca}_5(\text{PO}_4)_3\text{X}$; X = OH, F, Cl) is the most common phosphate mineral. Its hexagonal structure enables a large variety of substitutions, at the calcium (e.g., Sr^{2+} , Mn^{2+}), phosphorus (e.g., Si^{4+} , CO_3^{2-}), or channel sites (e.g., CO_3^{2-}) (Hughes and Rakovan 2002; Pan and Fleet 2002). It occurs in natural settings as diverse as igneous rocks, sedimentary deposits, or living organisms. Importantly, a carbonate-substituted hydroxyapatite (dahllite) is the major inorganic component of bones and dental enamel of vertebrates (Elliott 2002). Apatite is therefore a material of considerable biomedical importance (Gross and Berndt 2002). The preservation of the skeleton of fossil animals also provides important geochemical information about past environments and fauna paleoecology (e.g., Picard et al. 1998; Reynard et al. 1999; Sponheimer and Lee-Thorp 1999; Roche et al. 2010). Fluorapatite plays an important role in magmatic systems because it can host a number of elements that do not fit well in major rock-forming minerals (Piccoli and Candela 2002), whereas sedimentary deposits of carbonate-substituted fluorapatite (francolite) correspond to the principal natural resources in phosphorus (Knudsen and Gunter 2002). Finally, natural apatite is widely used for dating, using isotopic or physical methods (e.g., fission-tracks, electron paramagnetic resonance) (e.g., Ikeya 1993).

Important information about the structure of apatite samples can be obtained using vibrational spectroscopy. Infrared spectroscopy is routinely used to quantify the presence of carbonate ions in the structure and to assess the

E. Balan (✉) · S. Delattre · G. Morin · M. Guillaumet · M. Blanchard · M. Lazzeri · C. Brouder
Institut de Minéralogie et Physique des Milieux Condensés (IMPMC), UMR CNRS 7590, UMR IRD 206, Université Paris VI, Université Paris VII, IPGP, 140 rue de Lourmel, 75015 Paris, France
e-mail: Etienne.Balan@impmc.upmc.fr

D. Roche · L. Segalen
UPMC Univ Paris 06, UMR 7193 ISTEP, Biominéralisations et Environnements Sédimentaires, 75005 Paris, France

E. K. H. Salje
Department of Earth Sciences, University of Cambridge, Downing Street, Cambridge CB2 3EQ, UK

“crystallinity” of present or fossil biogenic apatite. Several “crystallinity” indices have been defined from the spectral features of the ν_4 PO_4 absorption bands occurring between 500 and 700 cm^{-1} (Rey et al. 1990; Shemesh 1990; Weiner and Bar-Yosef 1990; Surovell and Stiner 2001). They are widely used to assess diagenetic and fossilization effects in apatite (e.g., Michel et al. 1995, 1996; Pucéat et al. 2004; Lebon et al. 2010; Roche et al. 2010). In fact, these indices can be viewed as resolution factors and mostly depend on the width of the ν_4 PO_4 absorption bands. However, line profiles of vibrational absorption bands usually depend on various physical phenomena. Beside instrumental profile, the shape of infrared absorption bands results from the convolution of an intrinsic line profile (due to lifetime of the associated phonon) with a distribution function of phonon frequencies related to the system heterogeneity (Salje et al. 2000). In addition, long-range electrostatic effects may shift and modify the intensity of strong absorption bands in powder spectra, depending on the shape of the particles (e.g., Fuchs 1975; Ruppin 1977, 1978; Balan et al. 2001, 2008; Fourdrin et al. 2009). The comparison between various crystallinity indices obtained using various techniques, including infrared (IR) and Raman spectroscopy and X-ray diffraction, may lead to discordant results (Pucéat et al. 2004).

In the present study, we focus on the origin of line broadening in the powder infrared spectrum of fluorapatite and hydroxyapatite. Low-temperature infrared spectroscopic measurements make it possible to assess the respective contributions of homogeneous and inhomogeneous broadening, whereas a theoretical modeling is used to explore the relations between the particle shape and the powder absorption spectrum.

Experimental

Two synthetic fluorapatite and hydroxyapatite samples (Nounah and Lacout 1993) have been investigated. These samples contain trace amounts of cadmium ($\text{Cd}_{0.005}\text{Ca}_{9.995}(\text{PO}_4)_6(\text{F},\text{OH})_2$) and their mineralogical purity was checked by X-ray diffraction (Morin et al. 2002). Scanning electron microscope (SEM) observations (Fig. 1) show that the hydroxyapatite sample consists of lath-shaped particles with a length of ~ 200 nm and a thickness of ~ 40 nm. In contrast, the fluorapatite sample displays coalesced particles with a less well-defined shape. Pellets for infrared transmission measurements were obtained by pressing a mixture of about 1 mg of gently ground sample diluted in 300 mg of dried KBr. To improve the signal-to-noise ratio on the weak ν_1 PO_4 band, an additional series of low-temperature measurements was performed on more concentrated pellets with a sample/KBr ratio of 1 wt.%.

Transmission IR spectra were recorded between 500 and 4,000 cm^{-1} with a resolution of 1 cm^{-1} using a Nicolet 7600 FT-IR spectrometer. Low-temperature measurements between 10 and 270 K were performed using an ARS CS-204 SI cryocooler fitted with KRS-5 windows. Temperature was controlled using a Si diode fixed on the sample holder.

First-principles calculations

The vibrational properties of fluorapatite ($\text{Ca}_5(\text{PO}_4)_3\text{F}$) and hydroxyapatite ($\text{Ca}_5(\text{PO}_4)_3\text{OH}$) were computed within the density functional theory (DFT) framework, using the generalized gradient approximation (GGA) to the exchange–correlation functional as proposed by Perdew, Burke and Ernzerhof (PBE; Perdew et al. 1996). The ionic cores were described by ultrasoft pseudo-potentials from the Quantum Espresso library (<http://www.quantum-espresso.org>). The electronic wave functions were expanded in

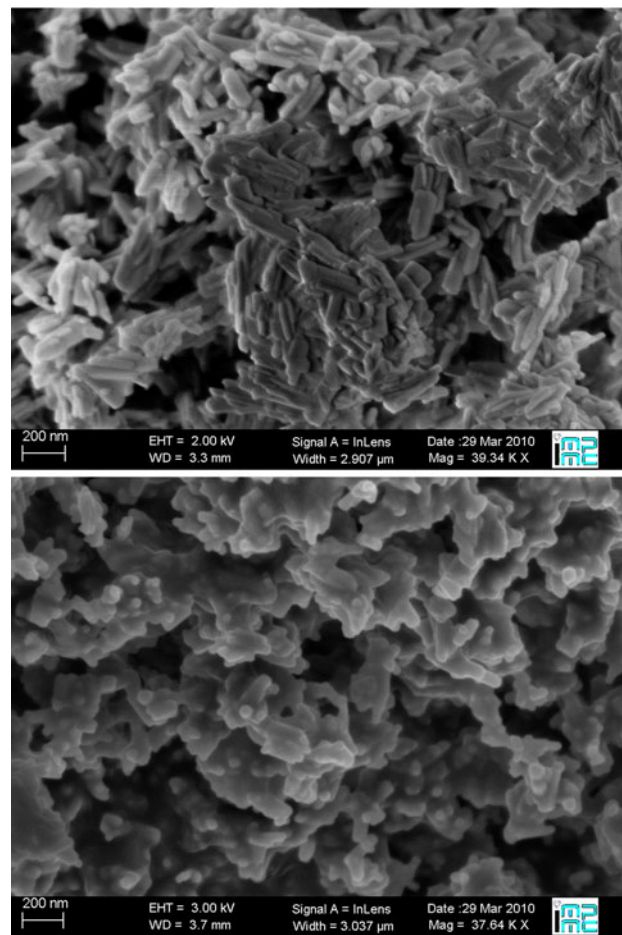
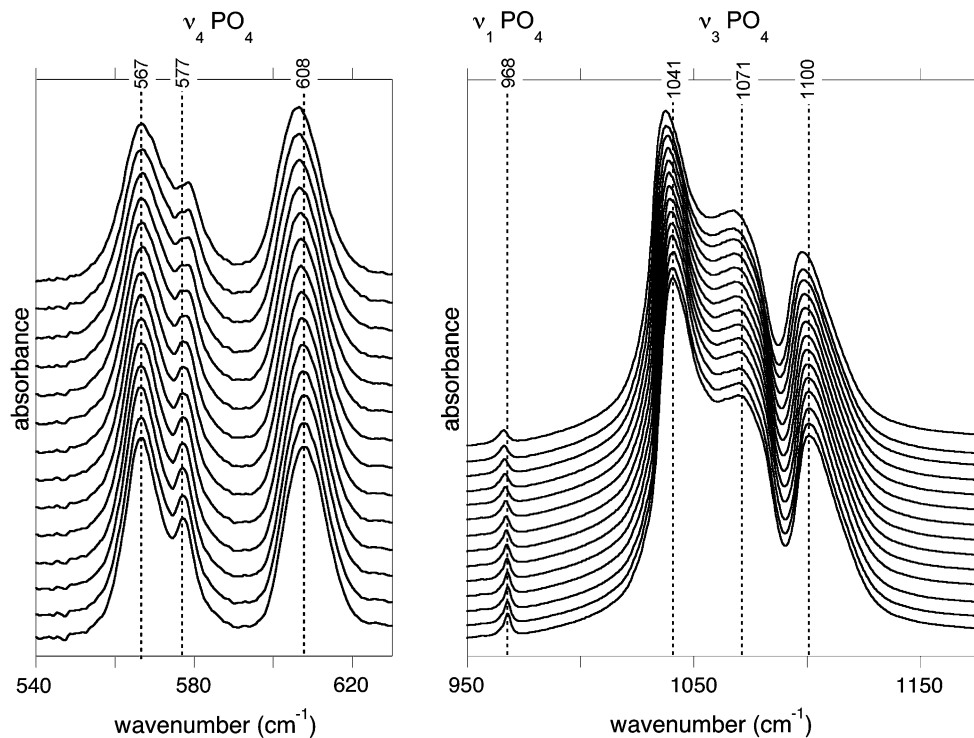


Fig. 1 SEM micrographs of synthetic hydroxyapatite (top) and fluorapatite (bottom) samples

Fig. 2 Powder transmission infrared spectra of fluorapatite from 270 (top) to 10 K (bottom) by steps of 20 K. Left $v_4 \text{PO}_4$ bands; right $v_3 \text{PO}_4$ and $v_1 \text{PO}_4$ bands



plane waves using a 40 Ry cutoff. A 380 Ry cutoff was used for the charge density. The electronic integration was performed by restricting the sampling of the Brillouin zone to a single k -point ($-0.5, -0.87, -0.68$) because of the relatively large unit cell of apatite (containing 42 and 44 atoms for fluorapatite and hydroxyapatite, respectively). The harmonic low-frequency dielectric tensor (Baroni et al. 2001) of the theoretical equilibrium structure was calculated using the PWscf and PHonon codes of the Quantum Espresso package (Giannozzi et al. 2009), following the procedure described in previous studies (e.g., Balan et al. 2001, 2005, 2008).

Results

Temperature dependence of apatite IR spectrum

The powder IR absorption spectrum of the investigated samples (Figs. 2, 3) displays the usual absorption bands of apatite (Farmer 1974). The bands observed above 500 cm^{-1} are related to internal vibration of the PO_4 tetrahedra. They are referred to as v_1 (symmetric stretch), v_2 (bending mode), v_3 (anti-symmetric stretch), and v_4 (bending mode) modes. Strong absorption bands associated with the $v_3 \text{PO}_4$ vibrations are observed between $1,000$ and $1,150 \text{ cm}^{-1}$. The much weaker $v_1 \text{PO}_4$ band is observed on the low-frequency side of the strong $v_3 \text{PO}_4$ band. Intense bands associated with the $v_4 \text{PO}_4$ vibration are observed between 540 and

620 cm^{-1} . Significant differences are observed between the hydroxyapatite and fluorapatite spectrum. As expected, two bands related to the stretching and bending of OH groups are observed in the IR spectrum of the hydroxyapatite sample at ca. $3,573$ and 630 cm^{-1} , respectively. More surprising, the spectrum of the hydroxyapatite sample displays a systematic splitting of the v_3 and $v_4 \text{PO}_4$ bands, which is not observed in the fluorapatite spectrum.

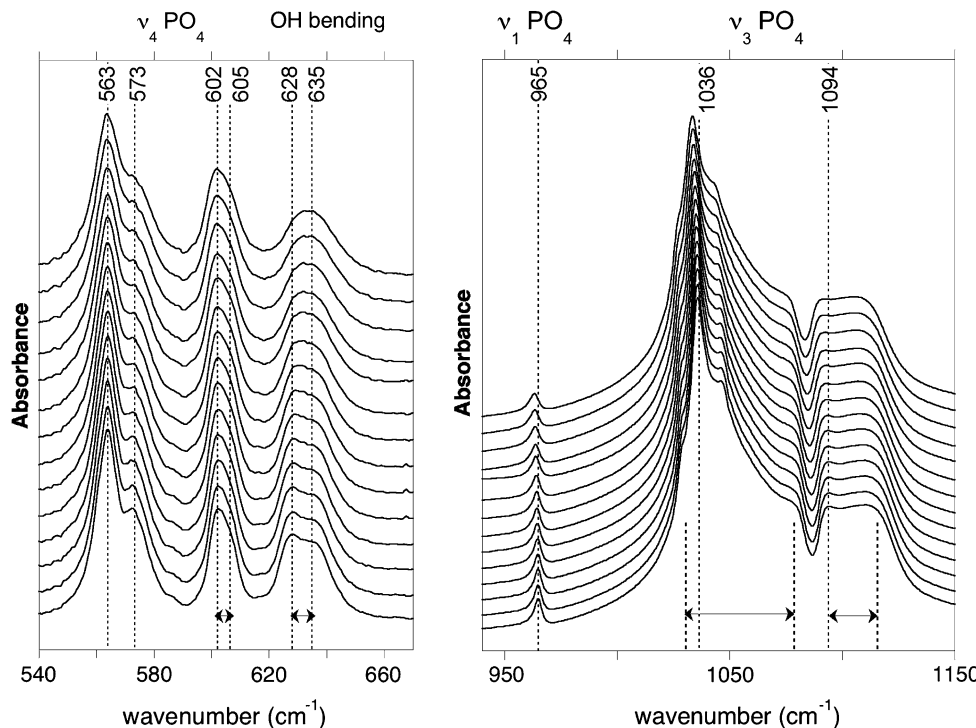
The lowering of temperature from 270 to 10 K leads to an overall narrowing of absorption bands and significant shifts are observed (Fig. 4). The shift of well-defined v_1 and $v_3 \text{PO}_4$ absorption bands is determined from the displacement of their maximum. Their frequency varies almost linearly with temperature above $\sim 100 \text{ K}$ but becomes temperature-independent at low temperature ($<\sim 100 \text{ K}$). The low-temperature quantum saturation of mode frequency is a general phenomenon in crystals and this behavior can be fitted using a function of the form (Salje et al. 1991a):

$$\omega(T) = A + B \coth(\Theta_S/T) \quad (1)$$

where T is the temperature. The A , B , and Θ_S parameters fitting the measurements are reported in Table 1. The “temperature-independent” domain extends from 0 to T_S with $T_S = \Theta_S/2$.

An overall increase in linewidth is observed as a function of temperature (Figs. 2, 3). The linewidth is extracted using an autocorrelation approach initially developed to investigate phase transitions in minerals using hard mode

Fig. 3 Powder transmission infrared spectra of hydroxyapatite from 270 (top) to 10 K (bottom) by steps of 20 K. Left v_4 PO₄ and OH bending bands; right v_3 PO₄ and v_1 PO₄ bands. Horizontal arrows point the line splitting related to the lath-shape of particles



spectroscopy (Salje et al. 2000). Compared to a fitting procedure, it does not require any assumption on the number of components or on the line shape. The self-convolution of the IR spectrum with an offset ω' in the frequency leads to the autocorrelation function:

$$\text{corr}(\alpha, \omega') = \int_{-\infty}^{+\infty} \alpha(\omega + \omega') \alpha(\omega) d\omega \quad (2)$$

where $\alpha(\omega)$ is the spectrum after baseline subtraction in absorbance units. The linewidth parameter (Δ_{corr}) is then obtained from the shape of the autocorrelation function in the limit $\omega' \rightarrow 0$ (Salje et al. 2000). It relates to the average linewidth and mode splitting in the relevant spectral region and proves to be rather more robust with respect to changes of baseline and instrumental noise than the usual line fitting procedure. For a Lorentzian profile, the extracted linewidth is close to the full-width at half-maximum. Practically, the method implies to choose some segments of the IR spectra and subtract a linear baseline in such a way that the intensity falls to zero at the limits of the segments, i.e., $\alpha(\omega) = 0$ beyond these limits (Table 1). Note that for overlapping lines such as the v_3 PO₄ bands, only an average parameter is obtained for the selected segment (975–1,175 cm⁻¹ for the v_3 PO₄ bands). At low temperature, the linewidth becomes also temperature-independent and the saturation behavior can be fitted using Eq. 1, as for the frequency shift (Table 1; Fig. 4).

The hydroxyapatite and fluorapatite spectrum displays similar shifts of the maximum of the v_1 and v_3 PO₄ bands as

a function of temperature. The slope of the curve in the linear domain, i.e., far from saturation, is given by the ratio B/Θ_S . Slopes of -1.5×10^{-2} and -1.3×10^{-2} cm⁻¹/K are observed for the v_3 band in fluorapatite and hydroxyapatite, respectively, whereas a slope of -0.93×10^{-2} cm⁻¹/K is observed for the v_1 band in both spectra.

Although both spectra display a low-temperature saturation of the linewidth, different slopes are observed in the high-temperature domain corresponding to linear variation of the linewidth. The width of the v_3 PO₄ band in the fluorapatite spectrum is larger, but its change as a function of temperature is weaker than its counterpart in the hydroxyapatite spectrum. Note that the broadening of v_3 PO₄ bands as a function of temperature is difficult to assess from visual inspection (Figs. 2, 3) but clearly appears as a result of the autocorrelation analysis. For the v_1 band, the broadening is visually clear (Figs. 2, 3). The slopes characterizing the changes in linewidth at high temperature (Fig. 4) are similar for both samples but the width at saturation is larger for the hydroxyapatite. Finally, the width of the v_4 band displays a similar behavior as a function of temperature, with a smaller width at saturation for the fluorapatite.

The frequency of the OH stretching absorption band in hydroxyapatite (Fig. 5) behaves similarly, with a saturation frequency of 3,574.5 cm⁻¹ and a slope of 1.35×10^{-2} cm⁻¹/K in the high-temperature linear domain. In contrast, the width of the band, which displays a Lorentzian line shape, is almost constant with a slight increase above 200 K. This suggests that the corresponding saturation

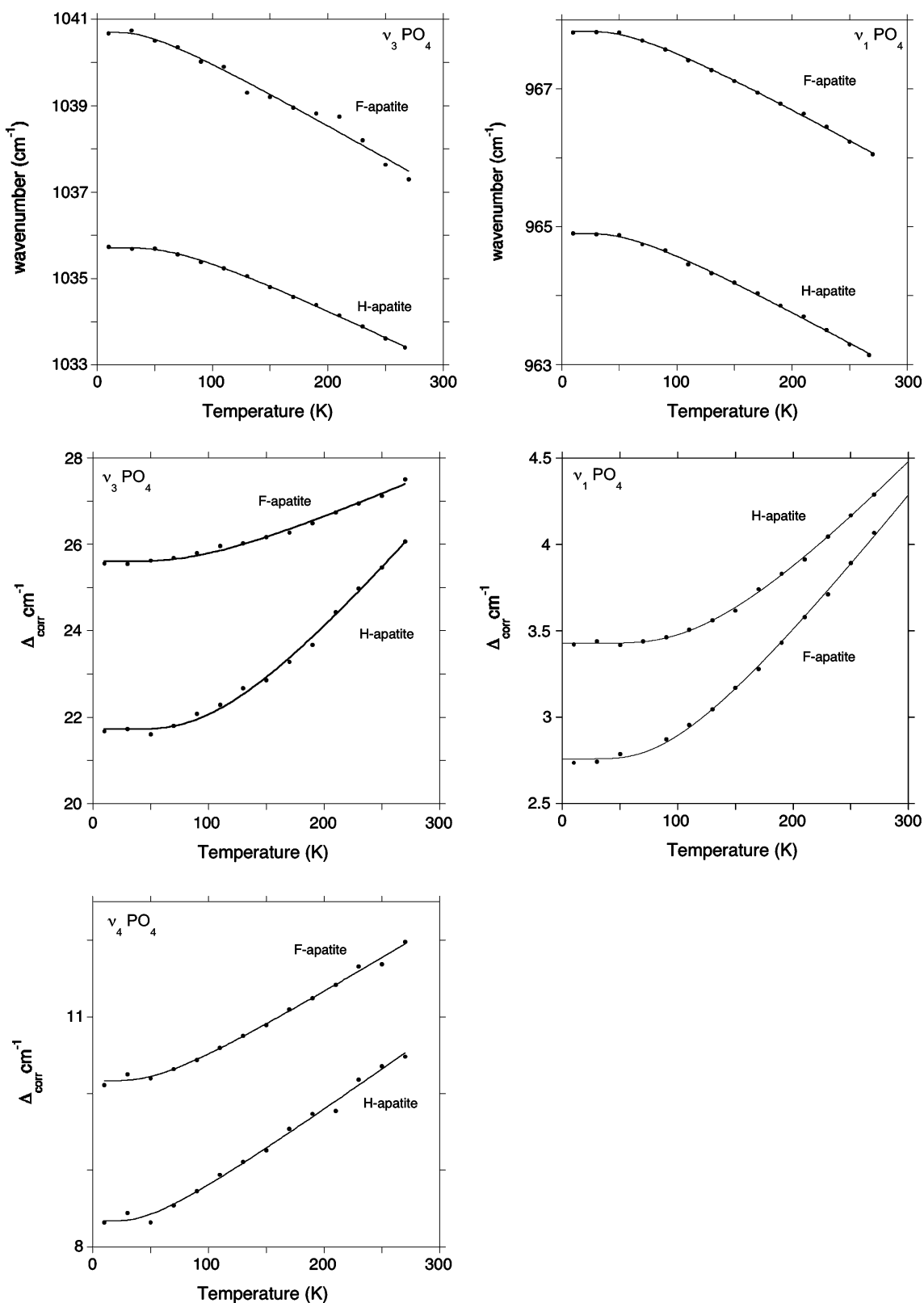


Fig. 4 Temperature dependence of the frequency and width of major PO_4 bands in the powder spectrum of apatite. The frequency is taken at the maximum of the absorption band and the width (Δ_{corr}) is

obtained by autocorrelation using the following domains 540–618 ($\nu_4 \text{PO}_4$, hydroxyapatite); 540–630 ($\nu_4 \text{PO}_4$, fluorapatite); 940–975 ($\nu_1 \text{PO}_4$) and 975–1,175 cm^{-1} ($\nu_3 \text{PO}_4$) (see text)

Table 1 Low-temperature saturation of the IR spectrum of apatite

		Θ_s (K)	A (cm^{-1})	B (cm^{-1})	B/Θ_s ($10^{-2} \text{ cm}^{-1}/\text{K}$)	Width at 0 K ^a
Frequency						
Hydroxyapatite	OH stretch	104	3,575.8	-1.4	-1.35	—
	$v_3 \text{ PO}_4$	106	1,037	-1.4	-1.32	—
	$v_1 \text{ PO}_4$	91	965.8	-0.85	-0.935	—
Fluorapatite	$v_3 \text{ PO}_4$	66	1,042	-1.0	-1.51	—
	$v_1 \text{ PO}_4$	93	968.7	-0.87	-0.935	—
Linewidth						
Hydroxyapatite	$v_3 \text{ PO}_4$	179	15.7	6.0	3.3	18.5
	$v_1 \text{ PO}_4$	211	1.8	1.62	7.7	2.6
	$v_4 \text{ PO}_4$	73	7.5	0.79	1.1	7.7
Fluorapatite	$v_3 \text{ PO}_4$	153	23.7	1.88	1.2	24.4
	$v_1 \text{ PO}_4$	152	1.4	1.34	8.8	1.9
	$v_4 \text{ PO}_4$	85	9.4	0.78	0.9	9.5

Parameters referring to Eq. 1
(see text)

^a The width at 0 K is obtained from a linear extrapolation of the high-temperature behavior

temperature Θ_s is probably above 400 K, significantly differing from that of phosphate bands.

Theoretical structural and vibrational properties of apatite

A number of studies have already investigated the theoretical structural and vibrational properties of apatite using empirical potentials or first-principles methods (e.g.,

Devarajan and Klee 1981; Lee et al. 2000; Haverty et al. 2005; Corno et al. 2006; Pedone et al. 2007). The agreement between theory and experiment is usually good, and calculated vibrational modes (Devarajan and Klee 1981; Corno et al. 2006; Pedone et al. 2007) confirm the interpretation of the vibrational modes observed above 400 cm^{-1} in terms of internal vibrations of the PO_4 tetrahedra. Some of these studies (Haverty et al. 2005; Corno et al. 2006; Pedone et al. 2007) suggest that a monoclinic

Fig. 5 Powder transmission infrared spectra of OH stretching mode in hydroxyapatite from 270 (top) to 10 K (bottom) by steps of 20 K. Right temperature dependence of the frequency and linewidth. Note the Lorentzian line shape of the absorption band

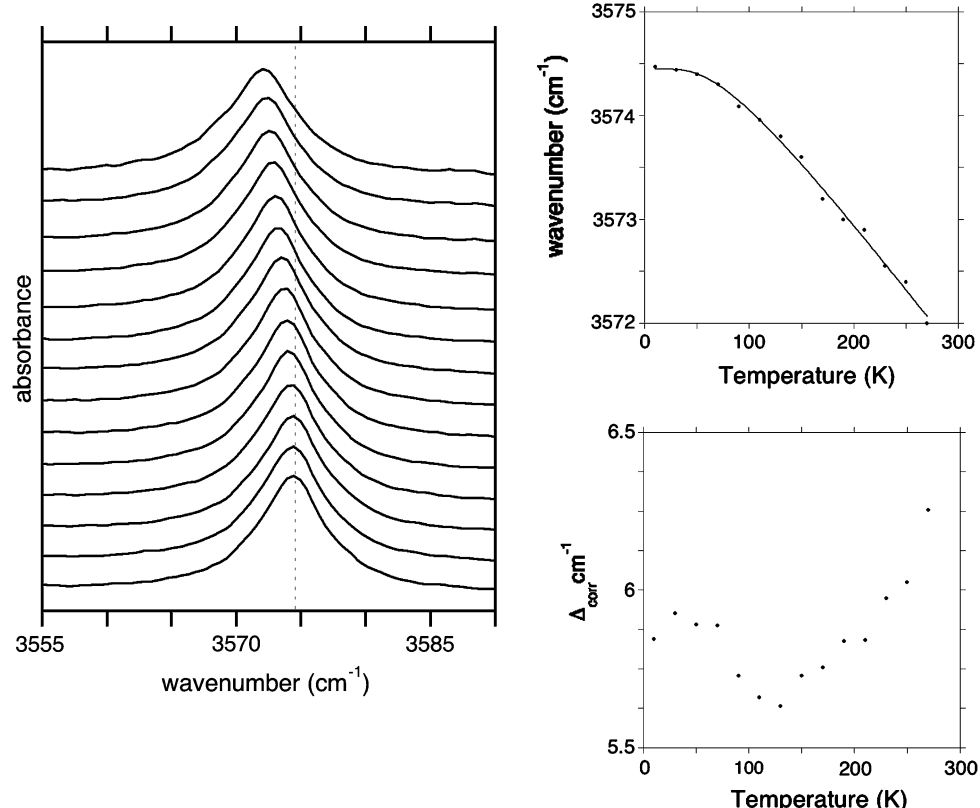


Table 2 Theoretical cell parameters, electronic dielectric tensor, and reduced atomic coordinates (below) of fluorapatite (S.G. P6₃/m) and hydroxyapatite (S.G. P6₃)

	Fluorapatite			Exp. ^a			Hydroxyapatite			Exp. ^a		
<i>a</i> (Å)	9.48			9.397	9.55					9.417		
<i>c</i> (Å)	6.90			6.878	6.87					6.875		
<i>c/a</i>	0.73			0.73	0.72					0.73		
ϵ_{∞} (<i>x, y</i>)	2.85			2.667	2.91							
ϵ_{∞} (<i>z</i>)	2.79			2.657	2.82							
Fluorapatite	<i>x</i>	<i>y</i>	<i>z</i>		Hydroxyapatite	<i>x</i>	<i>y</i>	<i>z</i>				
Ca(1)	0.67	0.33	0.00	Ca(1)		0.67	0.33	0.50				
Ca(2)	0.25	0.00	0.25	Ca(1)		0.33	0.67	0.50				
P	0.37	0.40	0.25	Ca(2)		0.25	0.25	0.75				
O	0.49	0.33	0.25	P		0.04	0.63	0.25				
O	0.47	0.59	0.25	O		0.09	0.74	0.06				
O	0.26	0.34	0.07	O		0.41	0.88	0.25				
F	0.00	0.00	0.25	O		0.66	0.92	0.43				
				O		0.84	0.51	0.25				
				O(H)		0.00	0.00	0.21				
				H		0.00	0.00	0.07				

^a Hughes et al. (1989)

structure of hydroxyapatite with space group P2₁/b, corresponding to an inverted orientation of OH groups in neighboring columns, would be slightly more stable than the ordered hexagonal structure with space group P6₃. Except for the orientation of OH groups, other properties, including vibrational frequencies are weakly affected by the change in the space group (Corno et al. 2006). In the present work, the modeling of hydroxyapatite was thus performed using the P6₃ space group, corresponding to a smaller unit-cell volume.

The theoretical, structural (Table 2) and vibrational (Table 3) properties of apatite obtained at the DFT–GGA level, in the present study, are mostly consistent with previous theoretical studies of apatite vibrational properties (e.g., Corno et al. 2006; Pedone et al. 2007) and will not be discussed in detail here. The relaxation of the fluorapatite and hydroxyapatite structures overestimates the *a* parameter by ~1% and reproduces the *c* parameter within 0.3%. Compared with experimental frequencies obtained from specular reflectance measurements on a single crystal of fluorapatite (Adams and Gardner 1974), the theoretical frequencies are softer by ~6%. Because of the smaller cell volume, the frequencies of the PO₄ stretching modes of fluorapatite are slightly higher (by a few cm⁻¹) than that of their counterparts in hydroxyapatite, consistent with the experimental observations. The OH bending and stretching frequencies in hydroxyapatite are calculated at 625 and 3,613 cm⁻¹, respectively.

Table 3 Transverse frequencies of IR-active zone-center vibrational modes of the equilibrium theoretical structures of apatite

	Theory (cm ⁻¹)	IR intensity	Exp. ^a
Fluorapatite			
<i>A</i> _u	90	m	96
	142	vw	–
	173	m	184
	238	vs	277
	268	s	304
	436	w	470
	523	s	582
	991	vs	1,030
<i>E</i> _{lu}	19	w	Lattice mode
	89	s	100
	166	vs	193
	203	vs	224
	227	vw	243
	250	s	273
	286	s	327
	437	w	460
	537	m	580
	564	s	604
	914	w	962
	989	vs	1,034
	1,047	m	1,094
Hydroxyapatite			
	Theory (cm ⁻¹)	IR intensity	
<i>A</i>	113	m	Lattice mode
	139	vw	–
	178	m	–
	203	vw	–
	215	vw	–
	243	vs	–
	254	m	–
	277	s	–
	445	w	v ₂ PO ₄
	527	s	v ₄ PO ₄
	991	vs	v ₃ PO ₄
<i>E</i> ₁	44	w	Lattice mode
	98	s	–
	128	w	–
	160	vs	–
	204	vs	–
	220	m	–
	228	m	–
	253	s	–
	276	vw	–
	321	s	–
	401	vw	–

Table 3 continued

Theory (cm^{-1})	IR intensity	
439	w	$\nu_2 \text{ PO}_4$
534	m	$\nu_4 \text{ PO}_4$
564	s	$\nu_4 \text{ PO}_4$
625	s	OH bending
913	w	$\nu_1 \text{ PO}_4$
985	vs	$\nu_3 \text{ PO}_4$
1,045	m	$\nu_3 \text{ PO}_4$
3,613	w	OH stretching

vs Very strong; s strong; m medium; w weak; vw very weak

^a Adams and Gardner (1974), Devarajan and Klee (1981)

The theoretical low-frequency dielectric tensor (Gonze and Lee 1997; Baroni et al. 2001; Balan et al. 2001) of fluorapatite and hydroxyapatite has been calculated using the vibrational modes, Born effective charge tensors and electronic dielectric tensor, as is usually done for polar solids (Tables 2, 3, Electronic Annexes). Infrared-active vibrational modes of apatite lead to the resonances observed in the dielectric tensor at the transverse optical frequencies (Fig. 6). These modes belong either to A or E_1 irreducible representations (A_u or E_{1u} for fluorapatite), corresponding to mode-polarization parallel or perpendicular to the c axis, respectively. In the case of perpendicular polarization (E_1 representation), two degenerate vibrational

modes occur with orthogonal polarizations. In the case of fluorapatite, the strong resonances related to the ν_3 PO_4 stretching modes and belonging to the E_{1u} and A_u irreducible representations occur at almost the same frequency, whereas a splitting can be observed for hydroxyapatite. There is a clear agreement between the resonances of the dielectric tensors and the observed absorption bands of the IR spectrum of apatite samples (Figs. 1, 2, 6).

Theoretical powder infrared spectrum of apatite

The determination of the low-frequency dielectric tensor makes it possible to investigate the role of a number of macroscopic parameters in the infrared spectrum of apatite. The low-frequency dielectric tensors of fluorapatite and hydroxyapatite are very similar, except for the additional bands related to OH vibrations in hydroxyapatite. Therefore, only hydroxyapatite will be considered in this part but the theoretical results will also hold for the internal vibrational modes of PO_4 tetrahedra in fluorapatite.

As usually observed for polar materials, the powder infrared spectrum of hydroxyapatite depends on the shape of the powder particles because of the long-range nature of electrostatic interactions. In this case, certain atomic vibrational modes can be coupled with a macroscopic electric field (i.e., constant over the unit cell), determined by the shape of the particles and by their low-frequency dielectric tensor (Balan et al. 2005). To investigate the relevance of these effects, the powder infrared spectrum of hydroxyapatite has been calculated for various particle shapes including spherical particles and needles elongated along the c axis (Fig. 7). Two different platy particles, perpendicular to the a axis or to the c axis, have also been considered. The powder spectrum is calculated by assuming that the particles are much smaller than the infrared wavelength and inserted in a homogeneous medium with the dielectric constant of KBr (taken equal to 2.25). The ingredients are therefore the ab initio dielectric tensor of apatite, the dielectric constant of the surrounding medium and the depolarization factors characterizing the particle shape (Balan et al. 2008). The absorbance spectrum is then proportional to the average power dissipated in the particle by the internal macroscopic electric field. This approach is equivalent to the modeling of the infrared absorption of a composite medium, made of mineral particles and diluting matrix, using the effective medium theory in the high-dilution limit (e.g., Yagil et al. 1995; Salje and Bismayer 1997; Balan et al. 2010).

Focusing on the frequency range of internal vibrations of phosphate and hydroxyl groups, the absorption bands calculated for a given particle shape can be significantly shifted with respect to the transverse optical frequencies of the corresponding vibrational modes. For a spherical

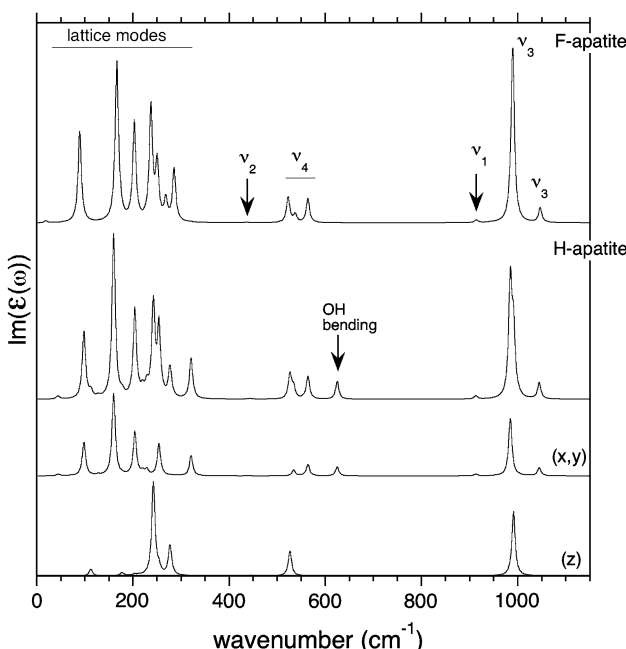


Fig. 6 Imaginary part of the theoretical low-frequency dielectric tensor of apatite. For hydroxyapatite, the contributions of A (z) and E_1 (x, y) modes are shown

particle, all bands are affected and larger shifts are observed for the most intense bands, which correspond to a stronger depolarization field in the particles. The relative intensity of the bands is also affected and some intensity transfer is observed from the lower to higher frequency bands with the same polarization. This is particularly evident on the two bands related to the v_3 PO₄ modes, whose relative intensity (Fig. 7) is significantly modified with respect to that of the corresponding resonances of the imaginary dielectric tensor (Fig. 6). For needles infinitely elongated along the c axis, the bands related to A modes, polarized along the c axis, occur at their transverse optical frequency. Only the bands related to E_1 modes, displaying a perpendicular polarization, occur at higher frequency. Because of the cylindrical geometry, no splitting occurs between the two degenerate E_1 modes. In contrast, platy particles infinitely extending along the b and c directions and infinitely thin along the a direction display a systematic splitting of the E_1 modes. The bands related to E_1 modes with a polarization along the b axis, together with those related to A modes, occur at their transverse optical frequency; whereas those related to E_1 modes but polarized

along the a axis occur at a higher frequency, coinciding with the longitudinal optical frequency (Balan et al. 2005). Finally, for platelets perpendicular to the c axis, the A modes are observed at the longitudinal frequency, whereas E_1 modes occur at their transverse frequency.

Discussion

In spectroscopy, the distinction between homogeneous and inhomogeneous broadening is often done on the basis of the shape of the line (Lorentzian or Gaussian, respectively). In the present case, this distinction cannot be used because the Lorentzian line shape in IR spectroscopy only corresponds to a significant simplification of the theoretical homogeneous profile (Salje et al. 2000). In addition, long-range electrostatic effects can strongly modify the profiles in powder spectra. In the following, we will assume that the homogeneous broadening is due to the anharmonic properties of the system and that the inhomogeneous one is due to sample imperfections and/or to the distribution of the particle shape in the composite sample. The temperature dependence of line profiles is thus used to make a distinction between homogeneous and inhomogeneous broadening contributions.

Homogeneous broadening and temperature dependence of the powder infrared spectrum of apatite

The shift and broadening of the infrared absorption bands as a function of temperature can be related to the anharmonic interactions (collision and scattering) between phonons, leading to frequency shifts and damping of vibrational excitations (e.g. Cowley 1968). While a detailed description of all the relevant processes requires quite demanding calculations (e.g., Menéndez and Cardona 1984; Lazzeri et al. 2003), the main characteristics of the shift and damping temperature behavior of a weakly anharmonic system can be described with a very simple model (Scott 1974). Using a complex damping constant α , the motion of a damped harmonic oscillator driven by an oscillating electric field of pulsation ω can be described by the equation:

$$m \ddot{X} + \alpha \dot{X} + kX = Z^* E_0 \exp(i\omega t) \quad (3)$$

where $\alpha/m = \Gamma + i\Delta$ and m , k and Z^* are effective mass, force constant and charge. Both Γ and Δ are proportional to the density of final states into which the phonon is decaying. Thus, they follow the Bose–Einstein occupation \bar{n}_i of the phonon states produced in the decay (Scott 1974):

$$\bar{n}_i = \frac{1}{\exp(\hbar\omega_i/k_B T) - 1} \quad (4)$$

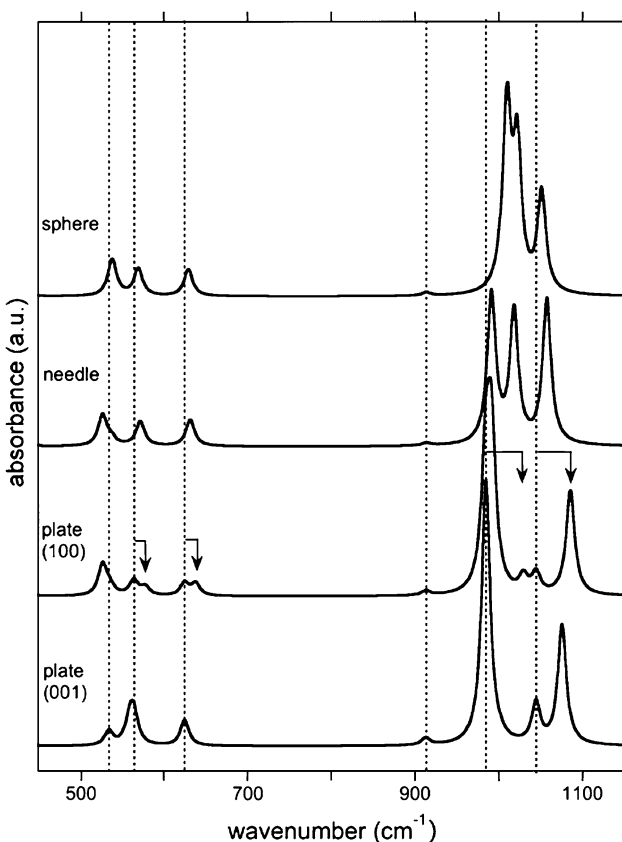


Fig. 7 Theoretical powder infrared absorption spectrum of hydroxyapatite calculated by considering various particle shapes (see text). The dotted lines correspond to the TO frequencies of E_1 modes. Arrows point the shape-related splitting of the E_1 bands for platelets perpendicular to the a axis

where ω_i is the phonon pulsation and k_B the Boltzmann constant. This dependence leads to the quantum saturation behavior observed at low temperature, which is conveniently fitted using Eq. 1. Leading terms in the frequency shifts are related to the third and fourth derivatives of the total energy with respect to atomic displacements (describing direct phonon collision events), and to the thermal expansion of the lattice, described by the mode Gruneisen parameter (e.g., Lazzeri et al. 2003). These various contributions may be of similar magnitude. In the present case, it is not straightforward to identify the dominant term. This would require, e.g., additional isothermal compression experiments (Samara and Morosin 1973). In contrast, the temperature dependence of the broadening is mostly related to the decay of the phonon into two other phonons. It thus depends on the anharmonic coupling of phonons in three-phonon interaction (scattering) processes, involving the third derivative of the total energy with respect to atomic displacements (e.g., Menéndez and Cardona 1984). The low saturation temperatures indicate that the internal vibrations of phosphate groups probe the average thermal bath of the crystal, without coupling to a specific decay channel (Salje et al. 1991b). When both the frequency shift and linewidth are considered for a given vibrational mode, the saturation temperature is usually higher for the linewidth, as previously observed in kaolinite-group minerals (Balan et al. 2010).

Interestingly, the stretching vibrations of OH groups in hydroxyapatite behave differently. Although the stretching frequency displays a saturation temperature similar to that observed for the phosphate modes, the linewidth display very weak variations. This observation suggests that coupling terms between the OH stretching vibrations and other vibrational modes of the crystal are very weak. This weakness might be related to the peculiar crystallographic location of OH groups at the center of structural channels, forming a linear chain of oscillators along the c axis.

Inhomogeneous broadening of the powder infrared spectrum of apatite

The linewidth obtained by extrapolating the high-temperature linear behavior to 0 K, i.e., by neglecting the quantum saturation, provides a direct assessment of the inhomogeneous broadening of the line, provided that the instrumental linewidth is small enough (Balan et al. 2010). Various factors can contribute to the inhomogeneous broadening of vibrational spectra. At a microscopic level, elastic strain related to the presence of defects or surface relaxation can lead to a distribution of vibrational frequencies. Macroscopic electrostatic effects can also play a significant role in the case of powder spectra. In that case, the vibrational frequencies are affected by the macroscopic

depolarization field, which occurs in the polarized particles. This field depends on the particle shape and will lead to an inhomogeneous broadening for distributed particle shape and/or non-ellipsoidal particles. For ordinary powder samples, the absorption bands are usually centered on a frequency close to that calculated for a spherical particle and the line broadening is of same order of magnitude as the splitting between the corresponding longitudinal and transverse optical frequencies. This interpretation is consistent with the larger average linewidth observed for the bands related to v_3 PO₄ modes ($>22\text{ cm}^{-1}$) than for those related to v_4 PO₄ modes ($\sim 10\text{ cm}^{-1}$). The v_3 PO₄ modes indeed display LO–TO splitting ranging between 40 and 80 cm⁻¹; whereas for the v_4 PO₄ modes they range from 10 to 30 cm⁻¹. This explains that the much weaker v_1 PO₄ bands with a very small LO–TO splitting ($<1\text{ cm}^{-1}$) also display the smaller linewidth ($\sim 3\text{ cm}^{-1}$). Importantly, these macroscopic electrostatic effects explain the splitting affecting specific absorption bands of the hydroxyapatite sample. Assuming that the elongation axis of lath-shaped particles is along the c axis, the anisotropic section leads to a stronger depolarization field when the mode-polarization is perpendicular to the lath plane than when it is parallel. This leads to two different vibrational frequencies, the higher being observed for the perpendicular orientation, instead of a simple line broadening centered on the spherical particle frequency. Note that the splitting cannot be ascribed to a lowering of the apatite crystal symmetry, which would affect both v_1 and v_3 PO₄ stretching bands. In comparison, electrostatic effects strongly modify the shape of the intense v_3 PO₄ bands; whereas the weak v_1 PO₄ stretching band is almost unaffected.

Infrared spectroscopic assessment of apatite crystallinity

The structural variations among apatite samples are often characterized by a modification of their crystallinity index, determined by the linewidth of the v_4 PO₄ bands (e.g., Rey et al. 1990; Shemesh 1990; Weiner and Bar-Yosef 1990; Michel et al. 1995, 1996; Surovell and Stiner 2001; Pucéat et al. 2004; Roche et al. 2010). As discussed above, the width of these bands is mostly related to inhomogeneous broadening effects, potentially involving both microscopic distortions of the crystal structure and macroscopic electrostatic effects, which are far from negligible for these bands. In contrast, the width of the weaker v_1 PO₄ band is weakly affected by electrostatic effects. It is dominated by microscopic parameters leading to homogeneous (through anharmonic coupling of phonons) and inhomogeneous broadening (when elastic strain related to defects or interfaces occurs). Therefore, the width of the v_1 PO₄ band should provide more accurate information on the

crystalline quality of apatite, than that of other stronger absorption bands. Noteworthy, the autocorrelation method is well suited to reliably extract the linewidth of the v_1 PO_4 absorption band, which may display an asymmetric line shape hardly fitted using Lorentzian or Gaussian functions. Finally, the vibrational bands observed in the Raman spectrum of apatite (e.g., Pucéat et al. 2004) are associated with a zero polarization and are therefore not affected by long-range electrostatic effects. It is thus possible to anticipate that the crystallinity parameters obtained from the width of v_1 PO_4 bands observed using IR or Raman spectroscopy should lead to a better consistency than those obtained using different vibrational modes.

Acknowledgments We thank Imene Machouk for her help in SEM observations. We gratefully acknowledge the technical support of F. Gélibart and M. Morand in the low-temperature measurements. This work was performed using HPC resources from GENCI-IDRIS (Grant 2009-i2009041519). Funding by the CNRS-INSU “INTERRVIE” program and UPMC “Emergence” program is acknowledged. This work is IPGP contribution 3048.

References

- Adams DM, Gardner IR (1974) Single-crystal vibrational spectra of apatite, vanadinite and mimetite. *J. Chem Soc Dalton* 14:1505–1509
- Balan E, Saitta AM, Mauri F, Calas G (2001) First-principles modeling of the infrared spectrum of kaolinite. *Am Mineral* 86:1321–1330
- Balan E, Lazzeri M, Saitta AM, Allard T, Fuchs Y, Mauri F (2005) First-principles study of OH stretching modes in kaolinite, dickite and nacrite. *Am Mineral* 90:50–60
- Balan E, Blanchard M, Hochepied J-F, Lazzeri M (2008) Surface modes of the infrared spectra of hydrous minerals: the OH stretching modes of bayerite. *Phys Chem Miner* 35:279–285
- Balan E, Delattre S, Guillaumet M, Salje EKH (2010) Low-temperature infrared spectroscopic study of OH stretching modes in kaolinite and dickite. *Am Mineral* 95:1257–1266
- Baroni S, de Gironcoli S, Dal Corso A, Giannozzi P (2001) Phonons and related crystal properties from density-functional perturbation theory. *Rev Mod Phys* 73:515–561
- Corno M, Busco C, Civalleri B, Ugliengo P (2006) Periodic ab initio study of structural and vibrational features of hexagonal hydroxyapatite $\text{Ca}_{10}(\text{PO}_4)_6(\text{OH})_2$. *Phys Chem Chem Phys* 8:2464–2472
- Cowley RA (1968) Anharmonic crystals. *Rep Prog Phys* 31:123–166
- Devarajan V, Klee WE (1981) A potential model for fluorapatite. *Phys Chem Miner* 7:35–42
- Elliott JC (2002) Calcium phosphate biominerals. In: Kohn MJ, Rakovan J, Hughes JM (eds) Phosphates geochemical, geobiological and materials importance. *Rev Miner Geochem* 48:427–453
- Farmer VC (1974) The IR spectra of minerals. Mineral Society, London
- Fourdrin C, Balan E, Allard T, Boukari C, Calas G (2009) Induced modifications of kaolinite under ionizing radiation: an infrared spectroscopic study. *Phys Chem Miner* 36:291–299
- Fuchs R (1975) Theory of the optical properties of ionic crystal cubes. *Phys Rev B* 11:1732–1740
- Giannozzi P, Baroni S, Bonini N, Calandra M, Car R, Cavazzoni C, Ceresoli D, Chiarotti GL, Cococcioni M, Dabo I, Dal Corso A, de Gironcoli S, Fabris S, Fratesi G, Gebauer R, Gerstmann U, Gougaudis C, Kokalj A, Lazzeri M, Martin-Samos L, Marzari N, Mauri F, Mazzarello R, Paolini S, Paolini S, Pasquarello A, Paulatto L, Sbraccia C, Scandolo S, Sclauzero G, Seitsonen AP, Smogunov A, Umari P, Wentzcovitch RM (2009) Quantum ESPRESSO: a modular and open-source software project for quantum simulations of materials. *J Phys Condens Matter* 21:395502
- Gonze X, Lee C (1997) Dynamical matrices, Born effective charges, dielectric permittivity tensors, and interatomic force constants from density-functional perturbation theory. *Phys Rev B* 55:10355–10368
- Gross KA, Berndt CC (2002) Biomedical applications of apatites. In: Kohn MJ, Rakovan J, Hughes JM (eds) Phosphates geochemical, geobiological and materials importance. *Rev Miner Geochem* 48:631–672
- Haverty D, Tofail SAM, Stanton KT, McMonagle JB (2005) Structure and stability of hydroxyapatite: density functional calculation and Rietveld analysis. *Phys Rev B* 71:094103–094109
- Hughes JM, Rakovan J (2002) The crystal structure of apatite, $\text{Ca}_5(\text{PO}_4)_3(\text{F},\text{OH},\text{Cl})$. In: Kohn MJ, Rakovan J, Hughes JM (eds) Phosphates geochemical, geobiological and materials importance. *Rev Miner Geochem* 48:1–12
- Hughes JM, Cameron M, Crowley KD (1989) Structural variations in natural F, OH, and Cl apatites. *Am Miner* 74:870–876
- Ikeya M (1993) New applications of electron spin resonance. Dating, dosimetry and microscopy. World Scientific Publishing Co. Pvt. Ltd., Singapore
- Knudsen AC, Gunter ME (2002) Sedimentary phosphates—an example: phosphoria formation, Southern Idaho, USA. In: Kohn MJ, Rakovan J, Hughes JM (eds) Phosphates geochemical, geobiological and materials importance. *Rev Miner Geochem* 48:363–389
- Lazzeri M, Calandra M, Mauri F (2003) Anharmonic frequency shift in MgB_2 . *Phys Rev B* 68:220509
- Lebon M, Reiche I, Bahain J-J, Chadeaux C, Moigne A-M, Fröhlich F, Sémaire F, Schwarcz HP, Falguères C (2010) New parameters for the characterization of diagenetic alterations and heat-induced changes of fossil bone mineral using Fourier transform infrared spectrometry. *J Archaeol Sci* 37:2265–2276
- Lee WT, Dove MT, Salje EKH (2000) Surface relaxations in hydroxyapatite. *J. Phys Condens Matter* 12:9829–9841
- Menéndez J, Cardona M (1984) Temperature dependence of the first-order Raman scattering by phonons in Si, Ge, and α -Sn: anharmonic effects. *Phys Rev B* 29:2051–2059
- Michel V, Ildefonse P, Morin G (1995) Chemical and structural changes in *Cervus elaphus* tooth enamels during fossilization (Lazaret cave): a combined IR and XRD Rietveld analysis. *Appl Geochem* 10:145–159
- Michel V, Ildefonse P, Morin G (1996) Assessment of archaeological bone and dentine preservation from Lazaret Cave (Middle Pleistocene) in France. *Palaeogeogr Palaeoclimatol Palaeoecol* 126:109–119
- Morin G, Allard T, Balan E, Ph Ildefonse, Calas G (2002) Native Cd^{+} in sedimentary fluorapatite. *Eur J Miner* 14:1087–1094
- Nounah A, Lacout JL (1993) Thermal behavior of cadmium containing apatites. *J Solid State Chem* 107:444–451
- Pan Y, Fleet M (2002) Compositions of the apatite-group minerals: substitution mechanisms and controlling factors. In: Kohn MJ, Rakovan J, Hughes JM (eds) Phosphates geochemical, geobiological and materials importance. *Rev Miner Geochem* 48:13–49
- Pedone A, Corno M, Civalleri B, Malavasi G, Menziani MC, Segre U, Ugliengo P (2007) An ab initio parameterized interatomic force field for hydroxyapatite. *J Mater Chem* 17:2061–2068
- Perdew JP, Burke K, Ernzerhof M (1996) Generalized gradient approximation made simple. *Phys Rev Lett* 77:3865–3868

- Picard S, Garcia JP, Lecuyer C, Sheppard SMF, Cappetta H, Emig CC (1998) $\delta^{18}\text{O}$ values of coexisting brachiopods and fish: temperature differences and estimates of paleo-water depths. *Geology* 26:975–978
- Piccoli PM, Candela PA (2002) Apatite in igneous systems. In: Kohn MJ, Rakovan J, Hughes JM (eds) Phosphates geochemical, geobiological and materials importance. *Rev Miner Geochem* 48:255–292
- Pucéat E, Reynard B, Lécuyer C (2004) Can crystallinity be used to determine the degree of chemical alteration of biogenic apatites? *Chem Geol* 205:83–97
- Rey C, Shimizu M, Collins B, Glimcher MJ (1990) Resolution-enhanced Fourier transform infrared spectroscopy study of the environment of phosphate ions in the early deposit of a solid phase of calcium-phosphate in bone and enamel, and their evolution with age. I. Investigations in the v4 PO₄ domain. *Calcif Tissue Int* 46:384–394
- Reynard B, Lécuyer C, Grandjean P (1999) Crystal-chemical controls on rare-earth elements concentration in fossil biogenic apatites and implications for paleo-environmental reconstructions. *Chem Geol* 155:233–241
- Roche D, Segalen L, Balan E, Delattre S (2010) Preservation assessment of Miocene–Pliocene tooth enamel from Tugen Hills (Kenyan Rift Valley) through FTIR, chemical and stable-isotope analysis. *J Archaeol Sci* 37:1690–1699
- Ruppin R (1977) Infrared absorption in sphéroïdal crystallites. *Surf Sci* 62:206–214
- Ruppin R (1978) Infrared absorption in rectangular crystallites. *Opt Commun* 26:360–362
- Salje EKH, Bismayer U (1997) Hard mode spectroscopy: the concept and applications. *Phase Transitions* 63:1–75
- Salje EKH, Wruck B, Thomas H (1991a) Order parameter saturation and low-temperature expansion of Landau theory. *Z Phys* 82:399–404
- Salje EKH, Wruck B, Marais S (1991b) Order parameter saturation at low temperatures—numerical results for displacive and O/D systems. *Ferroelectrics* 124:185–188
- Salje EKH, Carpenter MA et al (2000) Autocorrelation analysis of infrared spectra from minerals. *Eur J Miner* 12(3):503–519
- Samara GA, Morosin B (1973) Anharmonic effects in KTaO₃: ferroelectric mode, thermal expansion, and compressibility. *Phys Rev B* 3:1256–1264
- Scott JF (1974) Soft-mode spectroscopy: experimental studies of structural phase transitions. *Rev Mod Phys* 46:83–128
- Shemesh A (1990) Crystallinity and diagenesis of sedimentary apatite. *Geochim Cosmochim Acta* 54:2433–2438
- Sponheimer M, Lee-Thorp JA (1999) Alteration of enamel carbonate environments during fossilization. *J Archaeol Sci* 26:143–150
- Surovell TA, Stiner MC (2001) Standardizing infra-red measures of bone mineral crystallinity: an experimental approach. *J Archaeol Sci* 28:633–642
- Weiner S, Bar-Yosef O (1990) States of preservation of bones from prehistoric sites in the Near East: a survey. *J Archaeol Sci* 17:187–196
- Yagil Y, Baudenbacher F, Zhang M, Birch JR, Kinder H, Salje EKH (1995) Optical properties of YBa₂Cu₃O_{7-d} thin films. *Phys Rev B* 52:15582–15591